Composition and temperature-dependent magnetization dynamics in ferrimagnetic TbFeCo

Wei Li,[1] Jiaqi Yan,[1] Minghong Tang,[2] Shitao Lou,[1,*] Zongzhi Zhang,[2,†] X. L. Zhang,[1] and Q. Y. Jin[1,2,‡]
[1]*State Key Laboratory of Precision Spectroscopy, East China Normal University, Shanghai* 200062*, China*
[2]*Department of Optical Science and Engineering, Fudan University, Shanghai* 200433*, China*

(Received 16 November 2017; revised manuscript received 12 May 2018; published 30 May 2018)

The temperature-dependent magnetization dynamics in ferrimagnetic TbFeCo alloys with various compositions of Tb is investigated by the pump-probe time-resolved magneto-optical Kerr effect (TR-MOKE) in different geometries. It is shown that, for the case when a magnetic field is applied noncollinearly to the easy axis at room temperature, the decrease of the MOKE signal occurring at several tens of picoseconds (ps) after a rapid demagnetization within a few hundred femtoseconds (fs) is in fact caused by a highly damped precessional motion with precession lifetime shorter than the precession period. This is demonstrated by reducing the Tb content to 6% in atomic ratio and measuring TR-MOKE at elevated temperatures. This has the dual effect of reducing the damping constant allowing the observation of more precession cycles and of weakening the exchange interaction between Tb and FeCo, making the precession oscillations more pronounced. The results give important insight into the ultrafast spin dynamics of rare-earth-doped transition-metal alloys, and the remarkable impact of Tb on the damping in such alloy systems.

DOI: 10.1103/PhysRevB.97.184432

I. INTRODUCTION

In the past few decades, ultrafast magnetization dynamics in magnetic structures has attracted a great deal of attention due to its crucial importance for ultrafast magnetic recording and ultrafast spintronic devices [1–7]. Using an ultrashort laser pulse incident on magnetic films, the magnetization can be perturbed, showing an ultrafast demagnetization, in certain cases followed by a precession, and even a reversal of magnetization. The pioneering work by Beaurepaire *et al.* exploiting the time-resolved magneto-optical Kerr effect (TR-MOKE) on nickel thin films demonstrated an ultrafast demagnetization [1]. They introduced a phenomenological three-temperature (3T) model, describing the interaction between the electron, spin, and lattice subsystems and giving an explanation of the demagnetization and its relaxation. The ultrafast demagnetization of thin films consisting of only ferromagnetic transition metals (TMs) is considered to follow the 3T model with a demagnetization occurring at less than 1 ps.

In recent years, the magnetization dynamics of rare-earth–transition-metal (RE-TM) ferrimagnetic alloys such as GdCo, GdFeCo, TbFeCo, etc. has also been studied [6,7], and it has shown some different behaviors from that of ferromagnetic TM materials due to their complex magnetic structures. Mekonnen *et al.* presented their results of the laser-induced demagnetization in GdCo and GdFeCo [7], where they found a second demagnetization step. They proposed a four-temperature (4T) model to describe this phenomenon with four coupled differential equations that take the heat flow between the different heat baths (electrons, lattice, Gd $4f$ spins, and FeCo $3d$ spins) into consideration. The new observation of two-step demagnetization can then be well explained, with a result that the demagnetization of rare-earth (RE) metal is about two or three orders of magnitude slower than that of TMs [5,8–11]. In addition, some work including theoretical [12] and experimental [13–15] investigations has concerned the magnetization dynamics of precessional damping for RE-metal doped permalloy. It was found that most RE-metal atoms (such as Tb, etc.) induced a large increase of damping constant α except for Eu and Gd, which have no orbital momentum. Therefore, it is expected and also has been reported that the precession in RE-TM ferrimagnetic alloys with Tb, Dy, etc. rare-earth dopants ($>10\%$) is hardly observed, due to the very large increase of damping with those RE elements.

In RE-TM ferrimagnetic alloys, the magnetizations of RE and TM sublattices are aligned antiparallel and cancel each other at the magnetization compensation temperature T_{comp} [16]. The magnetic properties of RE-TM alloys, such as net saturation magnetization M_{s}, coercive field H_{c}, Curie temperature T_{c}, and T_{comp}, depend on Tb composition [16,17]. At T_{comp}, the net magnetization changes sign: below or above T_{comp}, the net magnetization is dominated by one of the magnetic sublattices (RE-dominant or TM-dominant).

To understand the magnetization dynamics of RE-TM ferrimagnets in more detail, we present here a careful and systematic study of the ultrafast demagnetization and relaxation of TbFeCo films, a typical RE-TM alloy with ferrimagnetic order. We investigate the magnetization dynamic behavior for different cases relative to T_{comp} by using Tb or FeCo-dominant alloys at room temperature (RT) and by changing the measurement temperature through T_{comp} at a given composition of Tb. The results show that when the magnetic field is applied noncollinearly to the easy axis, a magnetization precession takes place around the time range of

*stlou@admin.ecnu.edu.cn
†zzzhang@fudan.edu.cn
‡qyjin@phy.ecnu.edu.cn; qyjin@fudan.edu.cn

several tens of ps after a rapid demagnetization, with various damping constants depending on the Tb composition and temperature.

II. EXPERIMENTS

A. Samples

A series of amorphous thin films $Tb_x(Fe_{0.2}Co_{0.8})_{1-x}$ with various Tb compositions were deposited on Corning glass substrates in a Kurt J. Lesker magnetron sputtering system with a base pressure better than 1×10^{-8} Torr. The TbFeCo films were achieved by cosputtering from Tb and $Fe_{0.2}Co_{0.8}$ targets. A 4-nm-thick Ta layer was deposited on the glass as a buffer layer and a 6.7-nm-thick Pt on the top as a capping layer protecting the magnetic layer from oxidation. The thickness of TbFeCo is about 12 nm. All of the films were confirmed to have a perpendicular anisotropy by vibrating sample magnetometer (VSM) measurements in both in-plane and out-of-plane directions [18].

B. Measurement methods

The pump-probe TR-MOKE measurements were performed at various temperatures by a pulsed Ti:sapphire amplifier laser at a central wavelength of 800 nm, with a repetition rate of 1 kHz and a pulse width of about 130 fs. The linearly polarized laser beam was split into two parts with unequal powers, and the ratio of pump-to-probe beams was chosen to be approximately 40 : 1. The probe pulse beam was incident onto the sample at a small angle, and the spot sizes of the pump and probe beam are about 0.5 and 0.1 mm, respectively, so that homogeneous heating was ensured in the probing area of the sample. An external magnetic field H_{ext} generated by an electromagnet was applied at an angle of 17° with respect to the sample plane and perpendicular to the sample plane (i.e., parallel to the direction of magnetization). In these two configurations, the magneto-optical Kerr rotation was measured. The ellipticity was also measured to ensure that the optical (magnetization-independent) contributions to MOKE were negligible [19]. The signals were read out by a lock-in amplifier with an optical chopper that modulates the pump beam at a frequency of 108 Hz. We should mention that at a photon energy of 1.55 eV (800 nm in wavelength), the contribution to the magneto-optical Kerr signal is predominantly given by the FeCo subsystem [20,21].

III. RESULTS AND DISCUSSIONS

A. Static magnetic property measurements

The static magnetic properties were first measured by a vibrating sample magnetometer (VSM) at room temperature (RT). The sample with a Tb composition of 24% exhibits no obvious magnetic signal, which means the compensation temperature with 24% Tb is around RT, where the antiparallelly aligned Tb and FeCo magnetic sublattices compensate each other [22]. The samples with Tb compositions higher than 24% are Tb-dominant, and those having Tb compositions below 24% are FeCo-dominant. Figure 1(a) shows a variation of the

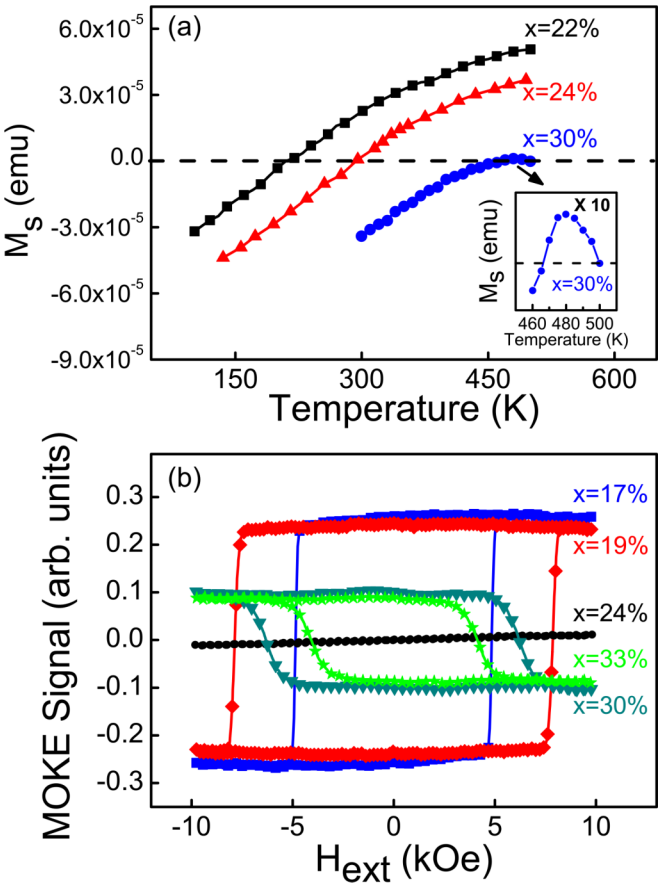

FIG. 1. (a) The saturation magnetization M_s as a function of temperature for $Tb_x(FeCo)_{1-x}$ ($x = 22\%$, 24%, and 30%). (b) The Kerr loops of MOKE without pump pulse for $Tb_x(FeCo)_{1-x}$ samples with various Tb compositions ($x = 17\%$, 19%, 24%, 30%, and 33%) at RT.

saturation magnetization M_s with temperature below 500 K for samples with $x = 22\%$, 24%, and 30% corresponding to FeCo-dominant, compensation composition, and Tb-dominant cases, respectively. Their T_{comp} are found to be 210, 295, and 470 K, respectively, and the measured Curie temperature T_c of the sample of $x = 30\%$ is about 500 K. No measurements were made beyond 500 K, but we would expect T_c for samples of 22% and 24% to be greater than this value. T_{comp} increases with increasing Tb composition, while T_c decreases [23]. Due to the strong intersublattice $3d$-$5d6s$-$4f$ exchange interaction between FeCo and Tb magnetic moments, T_c is higher than RT for TbFeCo alloys, though that of pure Tb is very low (only about 220 K [24]). The static magnetic properties were also measured using standard Kerr loops for all samples with various Tb compositions at RT [typical results are shown in Fig. 1(b)]. Clearly, the coercivity H_c increases close to the compensation composition of $x = 24\%$. The MOKE signal reverses when the composition increases through 24% (from FeCo-dominant to Tb-dominant, or vice versa) due to the change of direction of the FeCo magnetization. Moreover, magnetic hysteresis could not be observed for the concentration $x = 24\%$, which is attributed to its high coercivity (larger than our maximum magnetic field ~14 kOe).

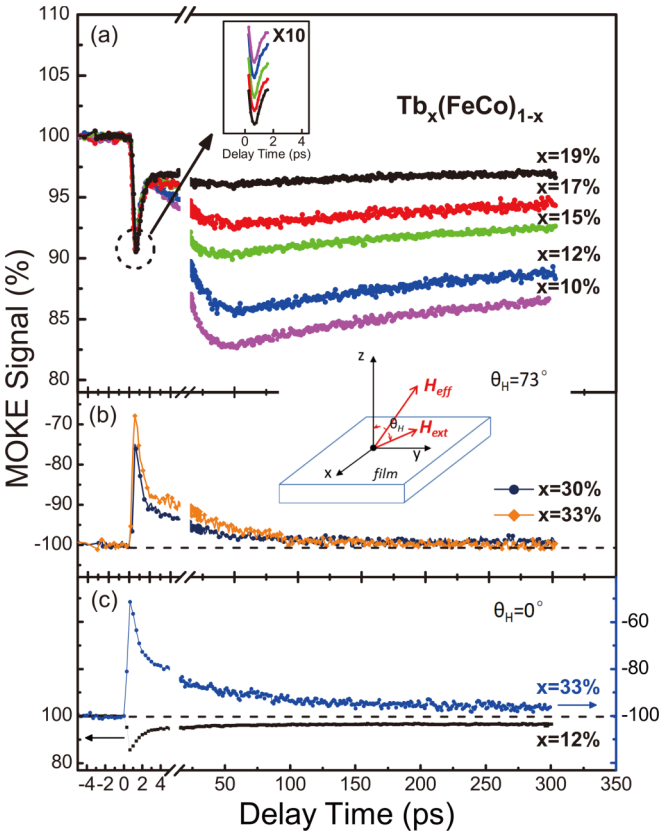

FIG. 2. TR-MOKE curves in $Tb_x(FeCo)_{1-x}$ using a pump fluence of 4.2 mJ/cm^2 with H_{ext} of 9.2 kOe at RT. (a) $x = 10\%$, 12%, 15%, 17%, and 19%; and (b) $x = 30\%$ and 33%. The orientation of magnetization (up or down) is decided by the external magnetic field. The inset between (a) and (b) shows the schematic illustration of the TR-MOKE measurement with H_{ext} applied with an angle θ_H of 73° away from the easy-axis direction of magnetization. (c) TR-MOKE curves at RT for samples of $Tb_{0.12}(FeCo)_{0.88}$ and $Tb_{0.33}(FeCo)_{0.67}$ in the polar geometry ($\theta_H = 0°$), i.e., H_{ext} is perpendicular to the film plane (parallel to the perpendicular anisotropy field of the films).

B. Composition-dependent magnetization dynamics

Figure 2 shows the TR-MOKE results of laser-induced magnetization dynamics with demagnetization and relaxation recovery in $Tb_x(FeCo)_{1-x}$ ($x = 10\%$, 12%, 15%, 17%, 19%, 30%, and 33%) using a pump fluence of 4.2 mJ/cm^2 under an external field of 9.2 kOe at RT. In Fig. 2(a), ultrafast demagnetization occurs initially at $\sim$ 600 fs. This process refers to the demagnetization of FeCo with a rapid increase of spin temperature of 3d electrons. Subsequently, a fast magnetization recovery takes place within about 2 ps, corresponding to the thermal equilibrium of the FeCo electron-spin-lattice system. With increasing Tb composition (from 10% to 19%), the amplitude of the demagnetization increases slightly [see the inset of Fig. 2(a)]. On changing from FeCo-dominant to Tb-dominant compositions, as shown in Fig. 2(b), the demagnetization amplitude for Tb-dominant samples is larger. The Kerr signal originates from the FeCo subsystem in TbFeCo alloys at a wavelength of 800 nm. In addition, the exchange interaction between FeCo spins is the most important factor to determine the demagnetization behavior, which is obviously Tb-composition-dependent. With the increase of Tb composition in TbFeCo, the demagnetization is thought to be easier due to the weakening of the exchange interaction between FeCo spins arising from the inhibition effect induced by Tb doping (T_c is also lower for higher Tb composition [23]). This is in accord with the result in Ref. [18], where it was found in TbCo alloys that the trend of magnetization quenching increased with increasing Tb composition because of the decreasing Co-Co coupling constant. In addition, another explanation of faster reduction of the signal with increasing Tb composition is the more efficient transfer of angular momentum between FeCo and Tb sublattices. The intersublattice angular momentum transfer speeds up the demagnetization in antiferromagnetically ordered materials [25].

After the ultrafast demagnetization and recovery processes within 2 ps, the curves exhibit an interesting phenomenon in that the Kerr signal decreases again. However, this phenomenon is not observed for Tb-dominant samples shown in Fig. 2(b). The schematic geometry for this TR-MOKE measurement is illustrated in the inset of Fig. 2. The external magnetic field H_{ext} is applied with an angle θ_H of 73° away from the easy-axis direction of magnetization (i.e., 17° relative to the film plane), driving the magnetization orientation away from the perpendicular easy axis. This geometry is set for the purpose of initiating the possible precession of magnetization when the external magnetic field is applied along the direction close to the hard axis of magnetization (with a small angle). This suggests that the second decrease of the Kerr signal might be related to the precession of magnetization.

To test this hypothesis, we carried out TR-MOKE measurements in a polar geometry, i.e., the magnetic field is applied perpendicular to the film plane (along the easy axis of magnetization for TbFeCo). Figure 2(c) gives the typical results for the samples with Tb compositions of 12% and 33%, where only ultrafast demagnetization can be observed for both FeCo-dominant and Tb-dominant samples. We did not find the second demagnetization described in GdFeCo with the same measurement geometry [7], because in TbFeCo alloys the angular momentum transfer from Tb magnetic moments to the lattice is considerably faster than that from Gd magnetic moments to the lattice in GdFeCo alloys, due to the nonzero 4f orbital momentum of Tb [9]. The second decrease of the Kerr signal occurring after 2 ps measured in the geometry of Fig. 2(a) is believed to correspond to the first oscillation of the magnetization precession of FeCo spins. Due to the very large damping constant in TbFeCo with rare-earth Tb atoms, the precession decays very fast and dies out before the completion of the first period of oscillation. This argument is also supported by the evidence of the magnetic-field-dependent TR-MOKE experiment. Figure 3(a) displays the TR-MOKE data for the sample of $x = 12\%$ using the same geometry as for the data in Fig. 2(a) with H_{ext} changing from 750 Oe to 14 kOe. The corresponding delay time of the minimum Kerr signal for the second decrease becomes smaller as H_{ext} increases, which is a typical feature of precession. Therefore, we believe that the dynamics occurring at several tens of ps timescale in Fig. 2(a) is the magnetization precession, which is sensitive to the applied magnetic field.

At the large delay (200–300 ps) shown in Fig. 2(a), the relative reduction of the MOKE signal is larger for smaller

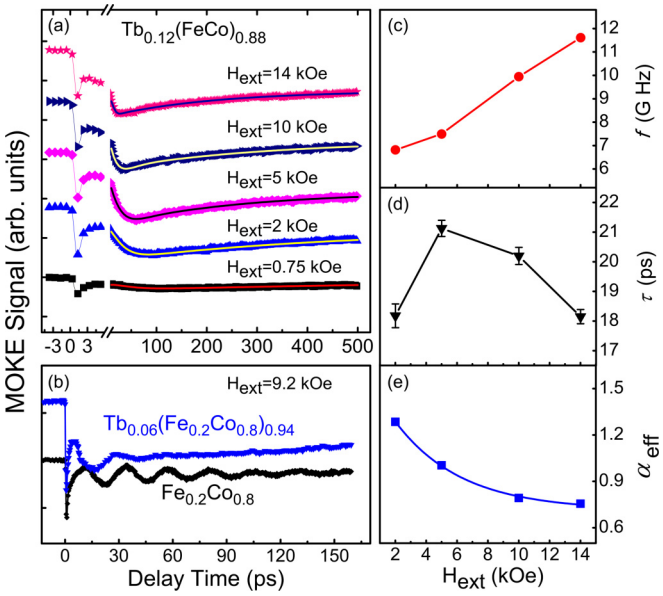

FIG. 3. TR-MOKE curves at RT as a function of H_{ext} for $Tb_{0.12}(Fe_{0.2}Co_{0.8})_{0.88}$ (a) for $Tb_{0.06}(Fe_{0.2}Co_{0.8})_{0.94}$ and pure $Fe_{0.2}Co_{0.8}$ (b). The solid lines in (a) are fitting curves. Parts (c)–(e) are, respectively, the magnetic-field dependences of magnetization precession frequency f, decay time τ, and the effective Gilbert damping α_{eff}, fitted from the TR-MOKE curves in (a).

Tb compositions. We know that at that delay, the precession is completely over, and the magnetization is oriented along the effective field direction. The relative reduction of the z projection of the magnetization is defined by the pump-induced tilt of the effective field, which reduces with increasing Tb composition. This could be caused by the relatively larger reduction of anisotropy field upon laser pumping for smaller Tb compositions, also it is possible due to the demagnetizing field effect when the external magnetic field is applied at an angle with respect to the sample plane. The demagnetizing field decreases with increasing Tb composition as a result of the smaller saturation magnetization for larger Tb compositions.

In addition, we know that Tb-doped FeCo films show a very strong dependence of the damping constant on the dopant composition. With increasing Tb composition, the damping constant α increases significantly [13,15]. We fabricated one sample with a low Tb composition of 6% and measured its dynamic curve at RT, as shown in Fig. 3(b), in which we see more precession oscillations than those with higher Tb compositions. As a comparison, the TR-MOKE curve of pure FeCo film is also displayed. Apparently, a very low Tb doping of 6% in FeCo has dramatically destroyed the precession, though still two precession oscillations could be identified. We fit the measured dynamic Kerr signal from Fig. 3(a) by using the following formula [26,27]:

$$\theta_k = a + be^{-t/t_0} + c\sin(2\pi ft + \varphi)e^{-t/\tau}, \qquad (1)$$

where the first term a corresponds to the background signal and it is close to zero. The second exponential decay term represents the slow magnetization recovery, where b is the amplitude and t_0 is the characteristic relaxation time. The third term describes the magnetization precession dynamics, where c, f, φ, and τ refer to the oscillation amplitude, frequency, initial phase, and decay time, respectively. The typical value of fit parameters a, b, c, and t_0 with H_{ext} of 10 kOe is 0.1, 0.07, 0.2, and 304.4, respectively. The fitted precession frequency f and decay time τ are, respectively, plotted in Figs. 3(c) and 3(d) as a function of H_{ext}. We obtain that the precession frequency f increases monotonically with H_{ext}. Based on the fitted f and τ, the effective Gilbert damping constant α_{eff} is derived approximately from the simple equation of $\alpha_{eff} = 1/2\pi f\tau$ [28]. As shown in Fig. 3(e), α_{eff} decreases dramatically with an increase of the external field H_{ext}. We can expect that by further increasing H_{ext}, the effective damping constant will eventually approach its intrinsic value. The high α_{eff} value in the low-field region results mainly from the inhomogeneous distribution of magnetization or magnetic anisotropy, which may arise from the interface roughness, thin layer thickness, and other factors [29].

We next utilize a decaying exponential function [29], $\alpha_{eff} = \alpha_{ex0}\exp(-H_{ext}/H_0) + \alpha_0$, to fit the α_{eff} data, where the extracted α_0 corresponds to α_{eff} at an infinite H_{ext}. The fitting curve is described by the solid line in Fig. 3(e), and the extracted α_0 is 0.714 ± 0.021, which is very close to the early experimental work for Tb-doped $Ni_{80}Fe_{20}$ [13]. In general, the origin of the increase of damping in TMs with RE impurities is based on the strong spin-orbit coupling or the spin-spin interaction. Theoretical work investigating orbit-orbit coupling between the conduction electrons and the impurity ions was presented by Rebei *et al.* [12]. But it was sharply contradicted by Woltersdorf *et al.*, who explained the temperature-dependent Gilbert damping by using the slowly relaxing impurity model [15]. Although these two models cannot be distinguished by the data in our paper, both of them reach the same conclusion, namely that the damping constant becomes large when RE is added in TM, which is consistent with the results in Fig. 2(b) showing that the precession damping of the Tb-dominant samples of 30% and 33% is so large that we cannot observe the occurrence of oscillation.

C. Temperature-dependent magnetization dynamics

As we mentioned at the beginning, in addition to the Tb composition change, measuring the TR-MOKE at various temperatures is another way to study the magnetization dynamics across T_{comp} (for some compositions of Tb). The compensation point T_{comp} of our $Tb_{0.24}(FeCo)_{0.76}$ sample is near RT. It goes to a lower temperature if Tb in TbFeCo becomes less, and it goes to a higher temperature in the opposite case. Studying temperature-dependent magnetization dynamics is also a way to change the exchange interaction between Tb and FeCo, which gives rise to a change in the precession damping constant. The temperature plays an important role in the precession damping [13].

Figure 4(a) shows the TR-MOKE signal dependence on the temperature for $Tb_{0.15}(FeCo)_{0.85}$. Its static MOKE curves without a pump pulse are shown in Fig. 4(b), where a reversal of the hysteresis loop is found at 80 K after crossing the compensation point ($T_{comp} \approx 100$ K). At RT, the precession starts but has not completed the first cycle, implying that the lifetime of precession is shorter than its period. This time we

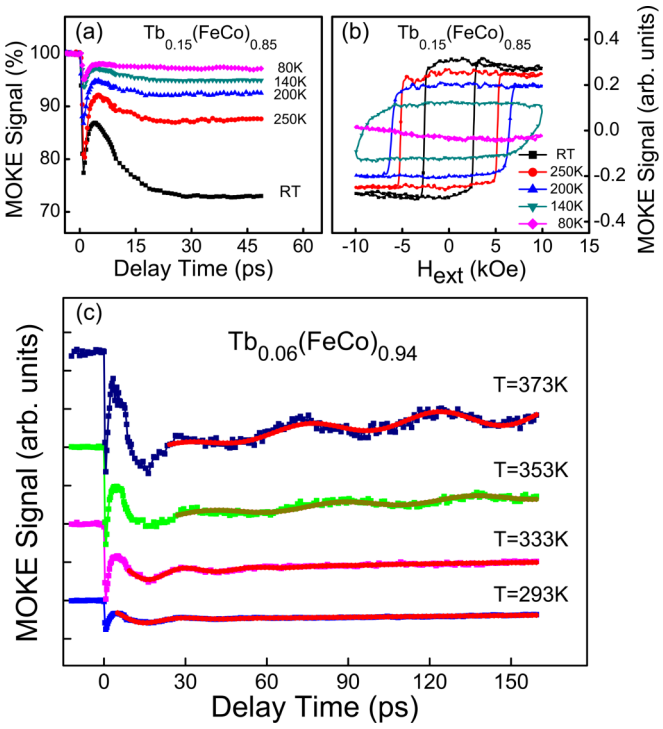

FIG. 4. (a) TR-MOKE curves measured at various temperatures for $Tb_{0.15}(FeCo)_{0.85}$ and (b) its static MOKE loops without a pump pulse. (c) TR-MOKE curves at various temperatures for $Tb_{0.06}(Fe_{0.2}Co_{0.8})_{0.94}$. Note that the sample temperature presented here does not include the temperature increase (roughly ∼40 K) induced by the pump heating.

use a higher pump fluence of 6.0 mJ/cm^2 in order to ensure that we can measure the precession for lower temperatures, thus the recovery seems more difficult than that with a lower pump fluence. At 200 K, we can still see the decrease of magnetization (part of the precession) to a minimal value at about 20 ps and a recovery afterward. But at 80 K, no clear precession could be distinguished. So, the precession becomes weakened as the temperature decreases from RT to 80 K, implying that the damping constant α increases with deceasing temperature. When we focus on the lower Tb composition of 6%, this phenomenon is revealed more clearly. Figure 4(c) shows the TR-MOKE results measured at various temperatures for the sample of $Tb_{0.06}(Fe_{0.2}Co_{0.8})_{0.94}$. Several complete oscillation periods of precession are clearly observed. The higher temperature leads to more precession oscillations. Normally we know that the scattering with magnons and phonons becomes stronger when the temperature increases, leading to a higher damping at higher temperature. Indeed, a phenomenon has been observed in Ref. [13] in which the damping constant α shows a small increase for undoped NiFe with increasing temperature. However, the NiFe sample with Tb doping exhibits a decreasing behavior in damping quite strongly with increasing temperature. The key point to explain this is the significant increase of damping originating from Tb dopants. When the temperature increases, the exchange interaction between Tb and FeCo becomes weaker [25]. Thus, the dissipation of precession energy becomes smaller since the efficiency of transfer of FeCo spin to the lattice through Tb magnetic moments reduces with increasing temperature, and the damping, which dominantly represents the dynamics of FeCo spins for TR-MOKE curves measured at a wavelength of 800 nm, will be lower at higher temperature. As a result, we observed a decrease of damping with increasing temperature.

IV. CONCLUSIONS

In summary, laser-induced ultrafast magnetization dynamics in the amorphous alloy TbFeCo is investigated by pump-probe TR-MOKE experiments. In the range of Tb composition from 10% to 33% in our samples, the amplitude of ultrafast demagnetization on a 1 ps timescale shows a slightly increasing trend with an increase of Tb composition. Moreover, if the magnetic field is applied noncollinearly to the easy axis at RT, the reduction of the MOKE signal occurring in tens of ps is a magnetization precession of FeCo spins, with a large damping constant when Tb composition is not very low. This is evidenced by the experiment with a magnetic field applied along its easy axis where the MOKE oscillation disappears. By changing the measurement temperature for the sample with a low Tb composition, we have found that the temperature plays an important role in helping to adjust the precession damping constant, so that we can see clear precession oscillations presented in TbFeCo alloys with less Tb composition at higher temperatures.

ACKNOWLEDGMENTS

This work was supported by the National Key R&D Program of China (2017YFA0303403), the National Basic Research Program of China (2014CB921104), the National Natural Science Foundation of China (Grants No. 11674095, No. 51671057, and No. 11474067), and the 111 project (B12024).

[1] E. Beaurepaire, J. C. Merle, A. Daunois, and J.-Y. Bigot, Ultrafast Spin Dynamics in Ferromagnetic Nickel, Phys. Rev. Lett. **76**, 4250 (1996).

[2] J. Hohlfeld, E. Matthias, R. Knorren, and K. H. Bennemann, Nonequilibrium Magnetization Dynamics of Nickel, Phys. Rev. Lett. **78**, 4861 (1997).

[3] A. Chekanov, K. Matsumoto, and K. Ozaki, Fluctuation field and time dependence of magnetization in TbFeCo amorphous rare earth-transition metal thin films for perpendicular magnetic recording, J. Appl. Phys. **90**, 4657 (2001).

[4] T. Ogasawara, K. Ohgushi, Y. Tomioka, K. S. Takahashi, H. Okamoto, M. Kawasaki, and Y. Tokura, General Features of Photoinduced Spin Dynamics in Ferromagnetic and Ferrimagnetic Compounds, Phys. Rev. Lett. **94**, 087202 (2005).

[5] B. Koopmans, G. Malinowski, F. Dalla Longa, D. Steiauf, M. Fähnle, T. Roth, M. Cinchetti, and M. Aeschlimann, Explaining

the paradoxical diversity of ultrafast laser-induced demagnetization, Nat. Mater. **9**, 259 (2010).

[6] Y. Ren, Y. L. Zuo, M. S. Si, Z. Z. Zhang, Q. Y. Jin, and S. M. Zhou, Correlation between ultrafast demagnetization process and Gilbert damping in amorphous TbFeCo films, IEEE Trans. Magn. **49**, 3159 (2013).

[7] A. Mekonnen, A. R. Khorsand, M. Cormier, A. V. Kimel, A. Kirilyuk, A. Hrabec, L. Ranno, A. Tsukamoto, A. Itoh, and Th. Rasing, Role of the inter-sublattice exchange coupling in short-laser-pulse-induced demagnetization dynamics of GdCo and GdCoFe alloys, Phys. Rev. B **87**, 180406 (2013).

[8] A. Melnikov, H. Prima-Garcia, M. Lisowski, T. Gießel, R. Weber, R. Schmidt, C. Gahl, N. M. Bulgakova, U. Bovensiepen, and M. Weinelt, Nonequilibrium Magnetization Dynamics of Gadolinium Studied by Magnetic Linear Dichroism in Time-Resolved $4f$ Core-Level Photoemission, Phys. Rev. Lett. **100**, 107202 (2008).

[9] M. Wietstruk, A. Melnikov, C. Stamm, T. Kachel, N. Pontius, M. Sultan, C. Gahl, M. Weinelt, H. A. Dürr, and U. Bovensiepen, Hot-Electron-Driven Enhancement of Spin-Lattice Coupling in Gd and Tb $4f$ Ferromagnets Observed by Femtosecond x-Ray magnetic circular dichroism, Phys. Rev. Lett. **106**, 127401 (2011).

[10] A. Vaterlaus, T. Beutler, and F. Meier, Spin-Lattice Relaxation Time of Ferromagnetic Gadolinium Determined with Time-Resolved Spin-Polarized Photoemission, Phys. Rev. Lett. **67**, 3314 (1991).

[11] A. Vaterlaus, T. Beutler, D. Guarisco, M. Lutz, and F. Meier, Spin-lattice relaxation in ferromagnets studied by time-resolved spin-polarized photoemission, Phys. Rev. B **46**, 5280 (1992).

[12] A. Rebei and J. Hohlfeld, Origin of Increase of Damping in Transition Metals with Rare-Earth-Metal Impurities, Phys. Rev. Lett. **97**, 117601 (2006).

[13] W. Bailey, P. Kabos, F. Mancoff, and S. Russek, Control of magnetization dynamics in $Ni_{81}Fe_{19}$ thin films through the use of rare-earth dopants, IEEE Trans. Magn. **37**, 1749 (2001).

[14] S. G. Reidy, L. Cheng, and W. E. Bailey, Dopants for independent control of precessional frequency and damping in $Ni_{81}Fe_{19}$ (50 nm) thin films, Appl. Phys. Lett. **82**, 1254 (2003).

[15] G. Woltersdorf, M. Kiessling, G. Meyer, J.-U. Thiele, and C. H. Back, Damping by Slow Relaxing Rare Earth Impurities in $Ni_{80}Fe_{20}$, Phys. Rev. Lett. **102**, 257602 (2009).

[16] T. A. Ostler, R. F. L. Evans, R. W. Chantrell, U. Atxitia, O. Chubykalo-Fesenko, I. Radu, R. Abrudan, F. Radu, A. Tsukamoto, A. Itoh, A. Kirilyuk, T. Rasing, and A. Kimel, Crystallographically amorphous ferrimagnetic alloys comparing a localized atomistic, Phys. Rev. B **84**, 024407 (2011).

[17] P. Hansen, C. Clausen, G. Much, M. Rosenkranz, and K. Witter, Magnetic and magneto-optical properties of rare-earth transition-metal alloys containing Gd, Tb, Fe, Co, J. Appl. Phys. **66**, 756 (1989).

[18] M. Tang, W. Li, Y. Ren, Z. Zhang, S. Lou, and Q. Y. Jin, Magnetic damping and perpendicular magnetic anisotropy in Pd-buffered $[Co/Ni]_5$ and $[Ni/Co]_5$ multilayers, RSC Adv. **7**, 5315 (2017).

[19] I. Razdolski, A. Alekhin, U. Martens, D. Bürstel, D. Diesing, M. Münzenberg, U. Bovensiepen, and A. Melnikov, Analysis of the time-resolved magneto-optical Kerr effect for ultrafast magnetization dynamics in ferromagnetic thin flms, J. Phys.: Condens. Matter **29**, 174002 (2017).

[20] A. R. Khorsand, M. Savoini, A. Kirilyuk, A. V. Kimel, A. Tsukamoto, A. Itoh, and Th. Rasing, Element-Specific Probing of Ultrafast Spin Dynamics in Multisublattice Magnets with Visible Light, Phys. Rev. Lett. **110**, 107205 (2013).

[21] S. Alebrand, U. Bierbrauer, M. Hehn, M. Gottwald, O. Schmitt, D. Steil, E. E. Fullerton, S. Mangin, M. Cinchetti, and M. Aeschlimann, Subpicosecond magnetization dynamics in TbCo alloys, Phys. Rev. B **89**, 144404 (2014).

[22] B. Hebler, C. Schubert, A. Liebig, M. Teich, M. Helm, M. Aeschlimann, M. Albrecht, and R. Bratschitsch, Thermally assisted all-optical helicity dependent magnetic switching in amorphous $Fe_{100-x}Tb_x$ alloy films, Adv. Mater. **25**, 3122-3128 (2013).

[23] S. Alebrand, M. Gottwald, M. Hehn, D. Stiel, M. Cinchetti, E. E. Fullerton, M. Aeschlimann, and S. Mangin, Light-induced magnetization reversal of high-anisotropy TbCo alloy films, Appl. Phys. Lett. **101**, 162408 (2012).

[24] M. Bode, M. Getzlaff, A. Kubetzka, R. Pascal, O. Pietzsch, and R. Wiesendanger, Temperature-Dependent Exchange Splitting of a Surface State on a Local-Moment Magnet: Tb(0001), Phys. Rev. Lett. **83**, 3017 (1999).

[25] J. H. Mentink, J. Hellsvik, D. V. Afanasiev, B. A. Ivanov, A. Kirilyuk, A. V. Kimel, O. Eriksson, M. I. Katsnelson, and Th. Rasing, Ultrafast Spin Dynamics in Multisublattice Magnets, Phys. Rev. Lett. **108**, 057202 (2012).

[26] H.-S. Song, K.-D. Lee, J.-W. Sohn, S.-H. Yang, S. S. P. Parkin, C.-Y. You, and S.-C. Shin, Relationship between Gilbert damping and magneto-crystalline anisotropy in a Ti-buffered Co/Ni multilayer system, Appl. Phys. Lett. **103**, 022406 (2013).

[27] P. He, X. Ma, J. W. Zhang, H. B. Zhao, G. Lüpke, Z. Shi, and S. M. Zhou, Quadratic Scaling of Intrinsic Gilbert Damping with Spin-Orbital Coupling in $L1_0$ FePdPt Films: Experiments and *Ab Initio* Calculations, Phys. Rev. Lett. **110**, 077203 (2013).

[28] G. Malinowski, K. C. Kuiper, R. Lavrijsen, H. J. M. Swagten, and B. Koopmans, Magnetization dynamics and Gilbert damping in ultrathin $Co_{48}Fe_{32}B_{20}$ films with out-of-plane anisotropy, Appl. Phys. Lett. **94**, 102501 (2009).

[29] M. Tang, W. Li, Y. Ren, Z. Zhang, and Q. Y. Jin, Lack of dependence between intrinsic magnetic damping and perpendicular magnetic anisotropy in $Cu(t_{Cu})[Ni/Co]_N$ multilayers, J. Magn. Magn. Mater. **428**, 269 (2017).